The Thesis Committee for Patrick Levi Jurney
Certifies that this is the approved version of the following thesis:

The Effect of Particle Size and Shape on Margination and Adhesion Propensity

APPROVED BY
SUPERVISING COMMITTEE:

Supervisor:

Li Shi

Krishnendu Roy

The Effect of Particle Size and Shape on Margination and Adhesion Propensity

by

Patrick Levi Jurney, B.S.M.E.

Thesis

Presented to the Faculty of the Graduate School of

The University of Texas at Austin

in Partial Fulfillment

of the Requirements

for the Degree of

Master of Science in Engineering

The University of Texas at Austin

August 2011

Dedication

To a better world

Acknowledgements

I would first like to thank my advisor and mentor, Prof. Li Shi, whose knowledge and patience are surpassed only by his benevolence in guiding me through this process. His input has been invaluable to my growth as a researcher and this contribution. I would also like to thank Prof. Krish Roy and Prof. S.V. Sreenivasan who have guided the growth of me and my project sagaciously over the past two years. I am also indebted to my fellow lab members, whose experience and insight has made this work possible.

I would like to thank the faculty and staff of the Microelectronics Research Center and the Cockrell School of Engineering as well as the countless professors, teachers, and coaches who have given their time teaching, training, and supporting me. I owe much of my remaining sanity to my friends who, over the years, have shown me the joy of exploration and the nobility of friendship, thank you. Finally, I would like to thank my mother, grandmother, father, stepmother, and siblings for their continued inspiration and support as I continue this wayward Jurney.

Abstract

The Effect of Particle Size and Shape on Margination and Adhesion Propensity

Patrick Levi Jurney, M. S. E.

The University of Texas at Austin, 2011

Supervisor: Li Shi

This thesis presents an experimental study of the effect that particle size and shape have on nanoparticle margination and adhesion propensity in micro-capillaries. With the use of half elliptical cross-section microfluidic channels that were fabricated using photolithography as well as wet and dry etching techniques and geometrically mimetic of human microcirculation, particles ranging from 93 to 970 nm were flown and imaged individually adhering to the channel walls. The results show a significant increase in particle adhesion below 200 nm as well as the emergence of a critical particle diameter above which no particle adherence was observed. The volume delivery efficiency was also shown to increase below 200 nm, providing insight for the rational design of nanocarriers for targeted cancer therapeutics.

Table of Contents

List of Tables

List of Figures

Chapter 1: Introduction

1.1 BACKGROUND

Traditional drug delivery approaches rely on exposing a sometimes lethal number of healthy cells to the cytotoxic drugs used in chemotherapy resulting in myelosuppression, immunosuppression, and all too often death. Recently, interest in a strategy for targeted drug delivery preferentially to the site of diseased cells based on rational design of drug-loaded nanoparticles has materialized. These drug-loaded nanoparticles or *nanocarriers* capable of moving laterally in vascular transport, recognizing diseased cells, firmly adhering, and delivering drugs preferentially to targeted cells appear a promising solution for the side effects associated with traditional cancer therapies. However, fundamental questions regarding the factors affecting vascular transport of nanocarriers still remain. The characterization of desirable properties such as a particle's propensity to marginate and adhere to a surface, particularly in a flow setup geometrically mimetic of human microcirculation remains elusive due to the difficulties associated with manufacturing and quantifying vast numbers of nanoparticles in microfluidic environments. This void and the potential benefit associated with a more profound understanding of such properties are the impetus for this work.

1.1.1 The Circulatory System

The closed loop circulatory system which supplies O_2 and other nutrients to tissues throughout the body, in addition to returning CO_2 to the lungs and metabolic biproducts to the kidneys for sequestration and filtration, serves to regulate corporal temperature and distribute agents that regulate cell function [1]. The process can be thought of to begin in the left ventricle of the heart. There blood, the working fluid of the circulatory system, a cellular smorgasbord of protein rich plasma, as well as red and white blood cells, and platelets; is pumped through a

bifurcating network of arteries and arterioles to the capillaries where it exchanges freely with interstitial fluid. This exchange occurs through pores and intracellular incursions in the endothelium. Table 1 shows typical diameter ranges for each quasi-circular cross-section blood vessel. Red blood cells have a characteristic size of 6-8 μm and due to their physical properties (i.e. size, shape, and compliance) flow preferentially in the center of blood vessels. This phenomenon is known as the *plasma skimming effect* [2].

Table 1: Sizes of various human blood vessels and corresponding cell free layer thicknesses.

Blood Vessel	Typical Diameter	Cell Free Layer Thickness
Vein	500 μm	Negligible
Artery	50-400 μm	Negligible
Arteriole	20-50 μm	8-15 μm
Venule	20 μm	6-20 μm
Capillary	5- 10 μm	5-10 μm

The direct result of the plasma skimming effect is the occurrence of a cell free layer adjacent to the endothelium, or vessel wall. The thickness of this cell free layer varies with both mean blood velocity and vessel diameter. Typical values for cell free layer thicknesses are shown in Table 1 for different blood vessels and were determined experimentally by Bugliarello and Sevilla [3] and Reinke et al. [4] as well as theoretically by Sharan and Popel [5]. For veins and arteries the cell free layer thickness is larger than arteries and arteriole but a negligible percentage of the total vessel diameter.

1.1.2 The Mononuclear Phagocyte System

The Mononuclear Phagocyte System (MPS) is a subsystem in the greater immune system comprised of vast quantities of phagocytic cells [6]. These cells, mainly macrophages and monocytes are found: lining the sinusoids of the liver, spleen, bone marrow and lymph nodes and serve to ‘gobble’ up particulate waste and potentially harmful agents in circulation. Note that in

past literature this system has been referred to as the reticuloendothelial system, however since most endothelial cells are not macrophages [7] MPS appears to be an increasingly canonical term. It is of paramount importance that a drug carrier effectively evades MPS sequestration, as macrophages pose an undesired destination for drug carriers in cancer therapeutics.

1.1.3 Diseased Tissue

The wall of all blood vessels is called the endothelium and is comprised of many endothelial cells packed in a fairly continuous and dense fashion. In cancerous tissue however, the tightly packed lining of endothelial cells that characterizes a healthy endothelium gives way to an increased number of inclusions, imperfections, and fenestrations with characteristic sizes as large as 2 μm [8, 9]. This feature was the impetus for a particle based drug delivery strategy known as the enhanced permeation and retention effect (EPR). The strategy is to load particles with therapeutic agents and exploit the fact that, being encapsulated in a larger carrier, the drugs will not extravasate in healthy tissue but preferentially in diseased vascular characterized by larger and more frequent fenestrations. In addition to the aforementioned microscale differences between healthy and diseased endothelia, cancerous cells have been shown to present a variety of surface receptors unique to cancer cells [10]. These receptors bind specifically with targeting ligands in a highly specific interaction and a vast number of potential receptor-ligand combinations are currently being explored as possible highly specific targeting mechanisms for deployment on the surface of nanocarriers [10, 11]. The average adult has a total capillary wall surface area of about 6300 m^2 [1]. The percentage of that area targetable for drug delivery in a tumor is dauntingly small for non-specific therapeutics and a more delicately tuned targeting approach is needed to increase drug efficacy as well as reduce the detrimental side effects typically associated with cancer therapies.

1.1.4 Margination

Margination is a term in physiology which refers to the lateral drift, typically of leukocytes and platelets but used here almost exclusively for nano and microparticles, from bulk blood vessel flow towards the endothelial walls. Particle margination is desirable for a myriad of reasons in nanotherapeutics. Whether employing an active vascular targeting approach or the passive EPR approach, particles in close proximity to the endothelium can interact with biophysical diversities such as the expression of specific receptors or large fenestrations through which to extravasate [12]. Bearing in mind that tumor vasculature is characterized by microcirculatory vessel diameters and tends to attach itself to healthy microcirculation; the other major advantage afforded to marginating particles is their ability to pass into increasingly smaller bifurcations in blood vessels which emanate from the walls of larger vessels. Differing from the active process which dictates leukocyte and platelet margination [13], nanoparticle margination can currently only be achieved through proper rational design [12] which requires a more profound understanding of the physics of nanoparticle margination.

1.2 Nano and Micro Particle Flow dynamics

Nano and micro particles exhibit complex behavior in microfluidic flow environments. Varying from random Brownian diffusion for the smallest of particles to gravitationally driven sedimentation for the largest, size is evidently an important factor governing vascular particle dynamics. Along with size, a whole host of other factors contribute to particle behavior including shape and density. In the following sections, the effects of buoyancy, size, shape, and other environmental factors on nano and micro particle vascular dynamics will be explored.

1.2.1 Neutrally buoyant spherical particles

Schonberg & Hinch showed that the migration of neutrally buoyant particles arises from the competition of two effects: one is due to the interaction between the particle and the wall,

while the other is due to shearing effects and the curvature of the velocity profile [14]. As a particle translates through the fluid it displaces fluid laterally. This displaced fluid eventually encounters the channel wall which retards further displacement and exerts a reactionary force on the particle perpendicular to the wall. If the particle is closer to one wall than another (i.e. not on the channel centerline) this effect results in a force toward the channel centerline. The other mechanism for particle migration discussed by Schonberg & Hinch arises due to the slower fluid velocity close to the channel wall compared to the centerline. As the particle displaces fluid, the difference between the displaced and background fluid velocities is greater on the channel wall side of the particle than on the centerline side. This velocity gradient produces a corresponding pressure gradient and subsequent particle margination toward the channel wall [15]. Goldman *et al.* eloquently described the motion of spherical particles submersed in a linear laminar flow [16]. A Neutrally buoyant spherical particle would tend to remain on a streamline and only marginate when a sufficiently large force acts with some component perpendicular to the streamline velocity. The hydrodynamic forces acting on the particle grow with particle size and some control of particle migration is possible by simply changing the size of neutrally buoyant spherical particles[17]

1.2.2 Non-neutrally buoyant spherical particles

Most polymeric nanocarriers, however, are not neutrally buoyant. The relative density between the fluid and particle can have an enormous impact on a particle's ability to escape streamline inertia. Gravitational forces have been shown to be relevant in spherical polystyrene particle migration down to diameters of ~500 nm [17]**.** In 1994, Hogg's seminal theoretical analysis described the channel migration of non-neutrally buoyant spherical particles in two-

dimensional shear flows. He characterized the problem using three non-dimensional groups [18]: the geometric parameter describing the ratio of the particle and channel length scales,

$$\alpha = \frac{d}{2l} \tag{1.1}$$

d and $2l$ being the particle diameter and channel height respectively; the channel Reynolds number,

$$Re_{channel} = \frac{\rho_f U_m R_{h,c}}{\mu} \tag{1.2}$$

where ρ_f is the density of the fluid, U_m the mean fluid velocity, μ the dynamic viscosity, $R_{h,c}$ the hydraulic radius of the channel given for a rectangular channel of width w by:

$$R_{h,c} = \frac{2lw}{l+w} \tag{1.3}$$

and finally a buoyancy number (B) which can be thought of as the ratio of the Stokes' settling velocity of the particle to the channel centerline velocity given by

$$B = \frac{d^2 \Delta\rho g}{18\mu U_m} \tag{1.4}$$

where $\Delta\rho$ is the density of the particle relative to the fluid and g is gravitational acceleration. Varying particle migration behaviors were identified dependent on the values of two non-dimensional parameters compared with unity:

$$\frac{\alpha^2}{B} \tag{1.5}$$

and

$$Re_{channel} B^2 \tag{1.6}$$

These regimes, shown in Table 2, correspond to the buoyancy of the particles and the relative importance of the particle and shear flow inertias. The regime where shear flow inertia is

dominant corresponds to viscous forces being balanced by advective terms in the region away from the particle due to undisturbed flow ($Re_{channel}B^2 \ll 1$) or, in other words, the forces acting perpendicular to the particle's streamline velocity are not sufficient to overcome the inertia keeping it flowing on the streamline. If however the dominant force balance away from the particle is that between viscous and inertial forces arising from particle motion then it is said to be the particle inertia regime ($Re_{channel}B^2 \gg 1$) and the particle's properties are sufficient to induce motion perpendicular to the streamline velocity.

Table 2: Flow regimes for spherical particle migration in shear flow

Flow Regimes	Neutrally Buoyant $\alpha^2/B \gg 1$	Non-neutrally Buoyant $\alpha^2/B \ll 1$
Shear Flow Inertia Dominant: $Re_{channel}B^2 \ll 1$	Particles marginate to non-centerline equilibrium distance from the wall [14].	Particles marginate to non-centerline equilibrium distance from the wall that is closer than for neutrally buoyant particles[18].
Particle Inertia Dominant: $Re_{channel}B^2 \gg 1$	No particle margination due to flow effects.	Particle migration toward the channel centerline [19].

Each of these regimes has been given significant treatment in a number of papers. As an example of the solutions given by Hogg, Vasseur & Cox, and Schonberg & Hinch; for relatively weak shear flows and slightly non-neutrally buoyant particles in a two dimensional shear flow the following scaling analyses give an idea of particle motion and the magnitude of the competing margination forces. The lateral motion of a non-neutrally buoyant particle is on the order of B with inertial corrections due to the curvature of the velocity profile on the order of $BRe_{Particle}^{\frac{1}{2}}$, and on the order of $\alpha Re_{Particle}$ due to the inertial interaction between displaced

fluid and the channel wall [18]. Order of magnitude analysis arising from first principles exists for all four of these regimes, for further discussion of scaling analysis and particle equilibrium positions for the range of cases discussed see Hogg, Vasseur & Cox, and Schonberg & Hinch [14, 18, 19].

The complex and bifurcating nature of the vessels comprising the circulatory system mean that not all vessels are aligned perpendicular with respect to gravity (horizontally). The margination behavior of non-neutrally buoyant spherical particles in planar boundaries oriented both horizontally and vertically for non-zero but small $Re_{channel}$ was described by Hogg [18] and has importance in designing marginating drug carriers. If the buoyancy of the particle is parallel to the flow direction (i.e. vertical channel orientation) then depending on the relative density of the particle, net motion toward or away from the wall will occur. The origin of this behavior is in the difference in relative velocities on the wall and centerline sides of a particle depending on whether that particle is traveling faster or slower than the surrounding fluid. If the particle is denser than the fluid i.e. the particle velocity is less than that of the undisturbed shear flow, then net particle migration toward the centerline will occur for the same reasons discussed for particle migration in horizontal channels. If the particle velocity exceeds that of the undisturbed shear flow then net margination toward the channel wall will occur. For example, an air bubble between two vertically oriented flat plates would tend to marginate towards the outer walls while a lead pellet of the same size would move preferentially toward the center of the channel.

1.2.3 Effect of Particle Size on Marignation and Adhesion Propensity

The effect of particle size on the margination and adhesion of non-neutrally buoyant particles in microflow environments can be profound. The size of a drifting particle affects not

only its in-flow dynamics but also its adhesion kinetics at the flow boundaries. The competing non-specific forces at the boundaries, most notably a shear detachment force and electrostatic interactions serving as non-specific adhesion forces, both increase with increasing particle size [20-22]. The nature of these coupled phenomena are such that attempts to describe the margination and adhesion behavior of micro and nano particles concurrently using numerical simulations have thus far been enlightened but insufficient. As a result, experimental determination of the effect size, shape, density, and surface characteristics have on the ultimate propensity of a particle to marginate and adhere in a vascular flow environment have begun to emerge as an exciting field of study with wide ranging impact.

In 2001 Patil *et al.* reported that for polystyrene microspheres from 5 to 20 μm in diameter, adhesion was a function of particle diameter and that with increasing shear rates, larger particles tend to adhere less than smaller ones. This observation points to the interplay between the shear detachment forces which are dependent on projected area in the flow direction and electrostatic interactions which, with respect to particle size, are dependent more readily on contact area.

In 2007 Decuzzi *et al.* demonstrated using a parallel plate flow chamber, a device consisting of either a Polymethyl methacrylate (PMMA) or Polydimethylsiloxane (PDMS) "floor" covered with a layer of cells, typically human umbilical vein endothelial cells (HUVECs), and a rubber gasket defining the flow volume with dimensions around 300 μm or more in height and several centimeters in both width and length, that for particles ranging from 500 to 10,000 nm, keeping the total volume of injected particle constant, the absolute number of particles adhering non-specifically decreases with the particle diameter according to the relation $d^{-1.7}$ and that the total volume of adherent particles per unit surface area increases with particle

diameter as $d^{1.3}$[23]. Meaning that for the size range between 500 and 10,000 nm, smaller particles marginate more than do larger ones on a per particle basis but interestingly, from a payload delivery metric, larger particles are more efficient delivery vehicles. However because of the *in-vivo* realities of mononuclear phagocyte particle sequestration as well as shearing induced particle detachment there is certainly a limit imposed on the efficiency gained by increasing particle size. Particle size becomes prohibitive in therapeutics when: i) the particles become too large to enter their blood vessels targets in microcirculation ii) the particle becomes larger than ~500 nm, below which EPR favors passive particle accumulation [24] or iii) the spherical particle exceeds ~200 nm in diameter and is at increased risked of recognition and sequestration by phagocytic cells in the MPS [25-27].

In 2008 Gentile *et al*. reported, using a similar parallel plate flow chamber, that two distinct regions of margination with respect to spherical polystyrene particle diameter exist: 500 to 10,000 nm and 50 to 200 nm. Keeping the total volume of injected particles constant, for larger particle diameters the margination behavior was shown to be governed mainly by the gravitational force. With the number of particles marginating per unit surface area and the corresponding total volume of marginated particles being dependent on particle diameter d and $d^{\frac{1}{4}}$ respectively. Keeping the number of particles injected constant and in contrast to particles with diameters > 200 nm, the total adhered particle volume per unit surface area of the smaller particles' could not be attributed to gravity and followed the relation $d^{3.2}$[28].

More recently in 2010 Charoenphol *et al.* reported, again using a similar parallel plate flow chamber and polystyrene spheres, the effects of particle size, shear rate, and channel height (vessel size), on margination and adhesion propensities. Particle sizes ranging from 500 to 10,000 nm, wall shear rates from 200 to 1500 s^{-1} (consistent with physiologically relevant shear

rates for this study [1, 29, 30]) and channel heights from 127 to 762 μm were implemented. Similarly to previous studies, particle adhesion at 200 s^{-1} was shown to increase with increasing particle size holding constant the volume of injected particles for each size. An interesting caveat reported was that converting the volume adhesion data per unit area back to total number of particles adhered and normalizing by the total number of particles injected also showed that particle margination efficiency increased with increasing particle diameter for these experimental conditions. This conclusion, however, is not without compounding variables, as the dependence of particle margination on concentration was not explored. It is possible that margination increases with increasing concentration as particle-particle interactions move particles off of streamlines and increase net outward particle inertia. The dependence of particle margination on wall shear rate showed an interesting trend which is discussed briefly above. The competition between adhesion and shearing forces rationalize the successive exclusion of smaller and smaller particles with increasing shear rates seen in this study. For example, given a particle diameter ≥ 2 μm, particle adhesion is shown to increase with increasing wall shear rate up to a "shear threshold" where it abruptly diminishes. For particle sizes smaller than 2 μm no such shear threshold was found for the shear rates considered even with the introduction of red blood cells which increased the appearance of such a threshold for larger particles[31]. Finally, the total particle flux at the wall was shown to increase with increasing channel height. However, when this was normalized by the total number of particles in the sedimentation volume (the volume of fluid directly above the imaged region) binding efficiency was found to decrease with increasing channel height. The authors attribute this to a possible decrease in red blood cell-particle interaction at the wall which, as shown in Table 1, is the result of increasing cell free layer thickness with increasing vessel diameter. Margination in vertical channels was also briefly

explored. A significant decrease in 5 and 10 μm diameter polystyrene particle adhesion in inverted channels is consistent with the theoretical work of Hogg [18] and is not explored further in this study. All other sizes showed similar trends to horizontally oriented channels which, again, points to the relatively weak effect gravity has on margination at increasingly small particle diameters [31].

More recently Toy *et al.* explored how size, as well as density and shape affect margination and adhesion propensities in nanoparticles. The results pertaining strictly to size will be discussed here and the effect of shape and density will be discussed in a later section. Using phosphate buffer solution (PBS) loaded liposomes with diameters of 130, 100, and 65 nm in a parallel plate flow chamber of height 175 μm, particle margination and adhesion propensity was determined using fluorescence intensity (see [32] for more details on the measurement methods). At a flow rate of 50 μl/min and fixed number of particles per solution volume, total particle margination and adhesion was found to increase with decreasing particle diameter. This experiment, well out of the previously discussed range where the gravitational force induces margination (> ~500 μm for polystyrene spheres), shows the emergence of a new regime in which diffusion through Brownian motion can be the dominant mechanism inducing margination. The ratio of species flux to its concentration gradient, or *diffusivity* is given by

$$\mathfrak{D} = \frac{k_B T}{3\pi\mu d} \tag{1.7}$$

Where k_B is the Boltzmann Constant and T is the absolute temperature. This quantity gives the diffusivity of a particle of a given size and is dependent on the inverse of the particle diameter. Given that gravitational forces can be neglected at this particle size scale and that diffusion is the

force driving particles off of streamlines and towards channel walls, it is consistent that smaller particles will have a higher propensity to marginate. Also noting that smaller particles have a reduced projected area and consequently minimized shear detachment force may offer some insight into the increased adhesion propensity, although these two phenomena were not decoupled here.

1.2.4 Effect of Particle Shape on Margination and Adhesion Propensity

To date, particularly relative to the effect of size, studies into the effect of particle shape on particle transport have been sparse [33]. Larger particles, with one dimension at least above the approximate limit for reduced MPS sequestration and often well above the threshold for preferential EPR extravasation, received more experimental attention due to the practicality in manufacturing larger particles. The effect of particle shape on the vascular transport of nanoparticles is a much more nascent field. Despite Jeffery's classical analytic solution for the effect of particle shape on the rheology of suspensions in 1922 [34], it wasn't until 2006 that Han *et al.* reported the effect of ellipsoidal particle aspect ratio on its diffusivity ($\mathfrak{D}$) both experimentally and theoretically [35]. Non-spherical particles exhibit an end-over-end tumbling behavior in microflow environments. This tumbling induces a complex periodic motion toward and away from channel walls. A number of attempts, both theoretical and experimental, have shed light on the complex marginating behavior of non-spherical non-neutrally buoyant particles. The attempts will be discussed in the following sections.

1.2.4.1 Modeling Techniques

The theory associated with the effect of shape on micro/nanoparticle vascular dynamics has thus far been largely a numerical modeling question. Not being able to describe exotic shapes' boundaries as constant values on an orthogonal coordinate system along with

enormously complex tensors arising from non-spherical particle tumbling mean that most work being done to describe the effect of particle shape on margination dynamics is in the field of numerical modeling. Immersed finite element method (IFEM), molecular dynamics, as well as dissipative particle dynamics are among the methods used to model the complex tumbling and adhering behavior of micro and nano particles.

In 2004 Decuzzi *et al.* proposed a mathematical model to predict the effect that hemodynamic conditions such as shear rate, viscoelastic considerations in ligand-recpetor bonds, and the density of surface ligands present on a particle's surface have on its adhesion propensity. Briefly, beginning with the classical relation

$$F(\dot{x}, x) = M\ddot{x} + nk_2\dot{x} + nk_1 \tag{1.8}$$

k_1 and k_2 being respectively the elastic and viscous parameters of the ligand-receptor system adhering the particle to the endothelial wall and *n* the number of active bonds. Neglecting inertial contributions ($M = 0$), a relation containing the propulsive force exerted by the fluid (kV_0) and the drag force over the particle ($-k\dot{x}$), having an absolute speed varying with time, emerges. The General solution for position, imposing the initial condition that the particle binds at terminal velocity ($\dot{x}(t = 0) = V_0$) is given by:

$$x(t) = \frac{kV_0}{nk_1}(1 + \frac{nk_1\tau}{k})\exp(-\frac{t}{\tau}) \tag{1.9}$$

with τ, the time constant for particle binding, being

$$\tau = \frac{nk_2 + k}{nk_1} \tag{1.10}$$

where k is the effective viscosity of blood. Adhesion force (F_A), or the force on a single ligand-receptor bond varies from zero at $t = 0$ up to the full propulsive force ($\frac{kV_0}{n}$) given by

$$F_A = \frac{kV_0}{n}(1 - \exp(-\frac{t}{\tau})) \tag{1.11}$$

Effectively the viscoelastic response of the whole system (including the particle, endothelial cell, and ligand-receptor bond) delays adhesion force growth rate ($\dot{F}_A$). While the propulsive force (kV_0) displays the opposite behavior: as propulsive force increases, maximum adhesion force and the corresponding growth rate of that adhesion force both increase, with $\dot{F}_A$ given by

$$\dot{F}_A = \frac{kV_0}{n\tau}(\exp(-\frac{t}{\tau})) \tag{1.12}$$

For rigid particle binding (e.g. that of a gold nanoparticle) the adhesion force F_A would grow from zero to $\frac{kV_0}{n}$ instantaneously. This is interesting because with no time-dependence the specific adhesion of rigid particles is shown to be a function solely of particle geometry (through the number of ligand-receptor sites) and vascular fluid properties. The effect of shear stress, loading rate, and ligand receptor density are also considered. Interestingly, high loading rate may activate several energy barriers and increase ligand-receptor binding rates leading to dramatic increases in adhesion probability. Both of these findings may be exploitable in the ration design of nanocarriers for increased efficacy[36].

Decuzzi *et al.* then developed a mathematical model to explore the effect of buoyancy, hemodynamic forces, van der Waals, electrostatic and steric interactions between a circulating particle and the vascular wall on the margination behavior of small particles. Only buoyancy, hemodynamic forces and van der Waals interactions were shown to affect particle margination[37].

The well known fluid-based resistance of a sphere in a quiescent fluid was given by Stokes as $3\pi\mu dv$. Balancing this settling resistance with a gravitational force acting downward, in a horizontally oriented channel, gives the simple relation for steady state settling velocity:

$$v_s = \frac{1}{18}\frac{g\Delta\rho}{\mu}d^2 \tag{1.13}$$

The effects of inertial fluid propagation toward the wall arise when the particle moves sufficiently close to the wall are not taken into account in this settling velocity. Solving the equation of motion in the direction perpendicular to the channel wall; for only hemodynamic forces which depend on the separation distance z between the particle center and the wall, the diameter of the particle, and the fluid viscosity; an expression for the product of hemodynamic resistance and falling velocity is given as

$$r(z)v_s = \frac{\pi}{6}gd^3\Delta\rho \tag{1.14}$$

with

$$r(z) = 3\pi\mu d\left[-\frac{1}{1-\frac{d}{2z}} + \frac{1}{8}\log(1-\frac{d}{2z})\right] \tag{1.15}$$

Several things are worth noting about this expression, namely that as the particle moves far away from the endothelium ($\frac{d}{2z} \to 0$) the resistance coincides with the Stokes resistance, and that for "heavy" particles ($\Delta\rho > 0$) the particle moves downward toward the endothelial wall in a horizontal channel and for light particles the opposite motion is predicted.

The next force considered is that arising from van der Waals interactions. For a detailed treatment of the nature of this and other intermolecular forces see Israelachvili's treatise [38]. The interaction energy between a small particle in a medium with an adjacent planar surface is given by the following equation

$$\omega_{vdW}(h) \cong -\frac{Ad^3}{24h^3} \tag{1.16}$$

With h being the distance between the particle and the endothelial wall ($z - \frac{d}{2}$) and A the Hamaker constant [38]. The derivative of the potential with respect to separation distance h gives the attractive van der Waals force

$$F_{vdW} = -\frac{\partial \omega}{\partial h} = A\frac{d^3}{8h^4} \tag{1.17}$$

The Hamaker constant can often be found explicitly and depends on the relative ability of each participating material to store charge, or dielectric constant. The dielectric constants of the particle (ε_p), channel wall (ε_w), and participating medium (ε_m) all effect the nature of the van der Waals force exerted on the particle and can even result in simultaneous particle attraction and repulsion. For instance, if $\varepsilon_m < \varepsilon_p < \varepsilon_w$ then the particle would be attracted to the wall from both sides. If we consider the wall to be the semi-permeable wall of an endothelial cell, then an interesting phenomenon would occur for the case where $\varepsilon_w < \varepsilon_m < \varepsilon_p$. In this case the particle would be attracted to the cell wall from the medium and upon binding to the surface, subsequently be repelled by the wall on the opposite side promoting particle internalization [37]. This observation may have a part to play in rational particle design for increased cytosis, which is the next hurdle in a nanocarrier's journey after successful margination and adhesion.

Forces arising from the formation of an electrostatic double layer and steric interactions of long polymer chains are also considered in this work but found to act only at very short distances from the wall (1-10 nm). The paper then derives the trajectories of numerous particles given the relations discussed above. They find that all particles settle toward the channel wall under the effect of gravity and exhibit a "jump into contact" behavior when h becomes small enough for van der Waals interactions to dominate particle motion. For a dimensionless separation distance ($\eta = 2h/d$) this jump into contact behavior dominates smaller particles at larger values of η. In other words smaller particles showed an increased relative propensity to

marginate and adhere than did larger particles. This analysis did show a critical radius at which the particle was large enough to marginate to the wall sufficiently quickly due to gravitational effects and small enough to jump into contact more readily than larger particles. This critical radius depends on $\Delta\rho$ as well as the electrostatic characteristics of the system but for physiologically relevant values and polymeric particles it is in the range of 100 nm [37].

Building on this spherical model Decuzzi *et al.* used a similar approach to describe the margination behavior of non-spherical particles in a linear laminar flow. Considering the effect of inertial and hemodynamic forces they showed that the torque arising from a particle's non-spherical geometry results a tumbling motion and can induce net lateral drift, or margination. Margination behavior for both micron and sub-micrometer sized particles of varying geometries were modeled. The propensity to marginate was reported in the form of a net lateral drift velocity and shown to be a function of both the Stokes number for a reference spherical particle:

$$St_d = \frac{\rho_p d^2 \dot{\gamma}}{4\mu} \tag{1.18}$$

and a normalized buoyancy parameter (G) similar to equation 2.4 but using a velocity length scale and particle diameter instead of the square of the particle diameter.

$$G = \frac{\Delta\rho g d}{\mu\dot{\gamma}} \tag{1.19}$$

A critical St_d for maximum margination at relative particle density of 2 and shear rate of 100 s^{-1} was found to be 0.1 below which no margination would occur up to a St_d of 20 where maximum drift velocity occurred. These values were found to be independent on both, particle shapes considered and values of G. Particles with the highest aspect ratio ($\gamma =$ particle height to width) were shown to have the highest margination propensity for all shear rates considered. Margination was also shown to increase with increasing shear rate and particle density [39].

This is of particular interest in microcirculation as relatively low shear rates are present and for moderate aspect ratios neither tumbling nor gravitational effects may be able to produce sufficient margination for nanotherapeutic delivery.

Up to this point the numerical modeling approaches focused on rigid particles of varying aspect ratio. However polymeric particles may exhibit deformability under physiological conditions. In order to couple the fluid domain of vascular flow regimes and the complex behavior of deformable solid particles, Liu *et al.* first reported the use of the Immersed Finite Element Method (IFEM) as a viable replacement for 1-D deformable modeling methods [40] and 2 or 3-D rigid models [41]. IFEM, developed by Zhang *et al.* [42] works roughly by coupling the boundary conditions at fluid-particle interfaces while maintaining finite element formulations for both the solid and fluid domains [43]. For a more detailed review of the computational specifics see the works by Liu *et al.* [43, 44] and Zhang *et al.* [42]. With relevance to this work, Liu *et al.* showed using IFEM that the tumbling behavior of non-spherical particles promotes adhesion and margination in several ways. For example, as a particle approaches the vessel wall it may contact it on either it's long or short axis. With the presence of conjugated ligands the particle will adhere specifically. Particles were shown to be *blown* over by the shearing fluid and *lay* with a low profile on the cell surface, significantly increasing the total adhering force due to increased contact area with the cell surface. This increase is greater for larger aspect ratios. Another advantage of high aspect ratio particle adherence was a decrease in the shear detachment force relative to that of a spherical particle of the same volume [45].

1.2.4.2 Experimental Determination

In 2007 Geng *et al.* used very high aspect ratio filomicelles, a highly stable di-block copolymer, to show that, in rodents, deviating from a spherical particle geometry to a high aspect

ratio formulation of identical composition increased circulation times *in-vivo* fourfold. The filomicelles were roughly cylindrical, having had a diameter of ~20-60 nm and ranging in length from 0.5-5 μm. The particles were shown to degrade over time, thus lowering the mean aspect ratio of a sample significantly through the course of the experiment. However larger initial length resulted in correspondingly longer circulation times. In a flow chamber experiment imploring phagocytotic cells (similar to those found in the MPS), spherical particles and segments of the filomicelles with lower aspect ratios were shown to be internalized by phagocytic cells more readily high aspect ratio particles [46].

Spherical particles of non-porous silica with diameter of 1 μm, discoidal polysilicon particles of height 0.3 μm and diameter 1.5 μm, and porous quasi-hemispherical silicon particles with diameters of either 1.6 or 3.2 μm were flown in a parallel plate flow chamber to determine the effect of shape and density on the margination propensity of potential drug carriers by Gentile *et al.* [47]. The total number of particles that marginated and adhered to the bottom surface of the flow chamber, with a height of 254 μm, was measured over time using bright field microscopy. A region of interest was used with dimensions of 276.48 x 276.48 μm^2 in which each adhered particle was counted in order to quantify the margination and adhesion propensities of each particle size at varying shear rates. The results were as follows: (i) the number of quasi-hemispherical silicon particles that marginated and adhered to the bottom surface decreased with the shear rate ($\dot{\gamma}$) following a power law $\dot{\gamma}^{-1}$ regardless of their density and size; (ii) the number of marginating spherical silica particles decreased with the shear rate $\dot{\gamma}$ with the scaling relationship $\dot{\gamma}^{-0.63}$; (iii) and the number of marginating discoidal polysilicon particles decreased with the shear rate $\dot{\gamma}$ according to the relationship $\dot{\gamma}^{-0.85}$. When comparing particles with similar weight, discoidal particles exhibited higher margination and adhesion propensities compared to

quasi-hemispherical and spherical particles. In a gravitational field, at a given shear rate (iv) denser particles marginate more than less dense particles and (v) large particles marginate more than small particles for the sizes explored in this study [47].

In 2010 Doshi *et al.* used what they branded "synthetic microvascular networks" (SMNs) to study the effect of shape on the vascular dynamics of particles ranging from 1-20 μm. SMNs are flow setups which are geometrically biomimetic of arteries or large arterioles (rectangular crosssection, but with dimensions of 100 x 50 μm^2). Using elongated spherical polystyrene particles they demonstrated that particle shape plays an important role in margination and adhesion propensities of microparticles in the given flow environments. The magnitude of this effect was notably dependent on the particle's aspect ratio. Polystyrene particles of varying geometries: spherical, circular disk, elliptical disk, or ellipsoidal were flown at a constant concentration of 5 x 10^5 particles/ml. Fluorescence images were taken after 180 s of flow and the number of particles adhered to the wall of the SMN reported as # of particles/cm^2. Elongated particles, elliptical disks and rods, consistently exhibited the highest propensities to marginate and adhere. Circular disks exhibited a lower propensity to marginate and adhere, while spherical particles were typically the least likely to exhibit such behavior. The SMNs used in this study had both a straight "inlet" portion and a bifurcating section wherein the 100 μm width of the channel gave way to two 50 μm sections at a separation angle of 90°. At this junction all particle adhesion for each of the 3 particle sizes considered: 1, 3, and 6 μm characteristic length, increased [48]. Mimetic of bifurucations present in human vasculature which eventually lead from large veins and arteries to progressively smaller vessels and eventually microcirculation, it is interesting that all particles tend to adhere more at these junctions. Implications may be that it is increasingly difficult for particles to navigate into microcirculation and tumor vasculature with

each bifurcation, but that once there will exhibit high delivering efficiencies and that increasing the aspect ratio of microcarriers may be favorable for treatment of diseases associated with angiogenesis.

Finally, in the most recent attempt to quantify the effect of particle shape on margination and adhesion propensity Toy *et al.* [32] explored the effect of nanoparticle shape, size, and density. Spherical liposomes loaded with either PBS or Iodine (diameters of 130, 100, and 65 nm), Iron oxide nanospheres (60 nm diameter), gold nanospheres, (60 nm diameter) and gold nanorods (length 56 nm and diameter 24 nm) were used in a flow setup similar to the SMNs described previously with a channel height and width of 100 and 175 μm respectively. Injecting particles at a constant concentration of 3×10^{11} particles/ml, each experiment was allowed to run for 8 minutes. As with all flow experiments of this nature some portion of injected particles adhered to the channel walls while some passed through the 5 cm channel without adhering. For each run, total intensity was measured using a fluorescence plate reader for the solution containing particles that passed through the channel and was collected at the outlet. The channel was then flushed with ethanol in order to remove the particles adhered to the channel wall and its fluorescence intensity measured. The volume of each sample was measured and the total number of particles in each portion calculated using a mass balance. This was then divided by the total number of particles injected over the course of the run to obtain a quantification of % particles adhered. For spherical liposomes of 65, 100 and 130 nm diameters respectively a general trend of increasing % adherence with decreasing particle diameter was observed consistent with the observations of Lee *et al.* [39] that at these size scales the contribution of buoyancy or gravity can be neglected and the dominate mechanism for margination is diffusion.

Liposomes loaded with PBS were assigned a relative density of 1 (ρ_{rp}= 1 g/ml), iodine (ρ_{rp}= 2.4 g/ml), iron oxide nanospheres (ρ_{rp}= 5.1 g/ml), and gold nanospheres (ρ_{rp}= 19.3 g/ml). These particles were all used to quantify the dependence of nanoparticle density on margination and adhesion propensity. All particles used in this study, having a diameter of ~65 nm, were well within the size range where diffusion is hypothesized to be the dominant mechanism of transport. This mechanism competes with the translational inertia of the particle keeping particles on flow streamlines. Therefore Toy *et al.* used a modified Peclet number to express the relative contributions of momentum and diffusion given by

$$Pe = \frac{Diffusion}{Momentum} = \frac{\mathfrak{D}}{\rho_{rp}/\rho_{water}} \times 10^{-4} \tag{1.20}$$

where $\mathfrak{D}$ is the diffusivity given by equation 1.7. Increasing this dimensionless quantity by adjusting ρ_{rp} led to a sizable increase particle margination and adherence.

Finally gold nanorods were compared with gold nanospheres in the first example to the author's knowledge of sub 100 nm nanoparticle shape affecting an *in-vitro* quantification of margination and adhesion propensity. An aspect ratio of ~2 (width and length 24 and 56 nm respectively) juxtaposed with a spherical particle of comparable size (60 nm diameter) showed an 8-fold increase in % adherence [32]. This result points to the profound effect shape may play in sub 200 nm nanoparticle transport.

The effect of size and shape of nano and micro particles on biodistribution in rats has been explored using polymeric particles of varying shapes and sizes with a significant trends reported [49]. However the dimensions of these particles were not small enough to i) avoid detection and sequestration by the MPS or ii) be considered diffusively dominated marginators. The reason these studies have not take place is that the ability to manufacture the number of particles needed for *in-vivo* studies with sufficient control of size and shape at sub 200 nm size

scales has yet to be demonstrated [33]. *In vitro* characterization of the effect of shape on margination and adhesion propensity offers an appealing stepping stone to eventually being able to rationally design nanocarriers to preferentially accumulate in desired tissue because much fewer particles are needed than for a full *in-vivo* study.

1.2.5 Other Factors Influencing Nanocarrier Transport

Beyond size and shape, surface charge and elastic modulus of nano and micro particles have an effect on their vascular dynamics. In 2011 DeSimone *et al.* fabricated biomimetic red blood cells of the biocompatible polymer polyethyleneglycol diacrylate (PEGDA). By varying the concentration of PEGDA they were able to tune the elastic modulus of the hydrogel microparticles from 7.8 to 63.9 kPa. Using these particles they performed an experiment to evaluate the effect a particle's elastic modulus on its ability to deform and traverse microcirculatory environments, and ultimately affect its biodistribution. It was shown that particles of lower elastic modulus were more capable of deforming to squeeze through narrow constrictions and thus make more resilient microcarriers. The effect of particle compliance *in-vivo* was explored using a biodistribution study. Rats were injected with synthetic red blood cells of varying elastic moduli and harvested 2h post-injection. Each organ was separated, weighed, and fluorescence signal quantified. When compared against controls, the biodistribution of each type of particle could be determined. They found that the elastic modulus of geometrically identical particles affected their ultimate biodistribution in a significant way, pointing to an affect both on particle-organ interaction and vascular dynamics. For example, decreasing the modulus of elasticity of these particles afforded them the ability to bypass several organs such as the lungs, which more rigid particles were not, resulting in longer circulation times *in vivo*[50].

Chapter 2: Experimental Methods

Marginating particles in vessels large enough to accommodate red bloods cells tend to accumulate in the cell free layer, where an almost linear laminar flow regime exists [12]. It is with this assumption that the parallel plate flow chamber has been employed with considerable success in studying margination and adhesion propensities of spherical particles [23, 28, 31, 32, 47]. However, in the microcirculatory environments of interest for turmeric payload delivery, a Poiseulle-like flow profile exits with either no red blood cells or, in the case of slightly larger capillaries, a single file parade of red blood cells. The physics of this environment and the complex interplay between nanoparticles, microparticles, and hemodynamic flow conditions may benefit from a more geometrically biomimetic experimental setup as the channel and particle Reynolds numbers both decrease.

2.1 Manufacturing Elliptical Cross-Section Microfluidic Channels

In order to manufacture half elliptical cross-section microfluidic channels, 100 mm diameter soda lime glass wafers 500 μm thick (University Wafer) were cleaned using a Piranha etch (37 % H_2O_2: 96 % H_2SO_4 = 1:2 by volume) for 8 minutes followed by a 20 s diluted Hydrofluoric Acid bath (H_2O: HF = 200:1 by volume) to removed native oxide. A schematic of the fabrication process is shown in Figure 2.1. Next, 700 nm of Cr was deposited using a CHA Metal Evaporator. Then hexamethyldisilazane (HMDS) was vapor coated onto the sample in order to promote adhesion of the photoresist layer to come. In order to reduce streak formation, AZ 4330-RS positive photoresist was spun from 0 to 4000 RPM at a ramp rate of 200 RPM/s for 20 s then held at 4000 RPM for 30 s resulting in a 3.4 μm thick layer. The sample was then soft baked at 90 °C for 60 s and patterned using a Karl Suss MA6 Mask Aligner at a constant power of 274 W for 17 s. The sample was then developed in AZ 400K Developer diluted 1:4 in H_2O

for 210 s. A hard baking procedure was then performed in an oven at 115 °C for 60 s and allowed to cool to room temperature for 30 minutes in order to minimize thermal shock on the photoresist and prevent crack formation. The Cr layer was then etched using a Trion Oracle RIE etcher with Cl_2 and O_2 flown at 40 and 10 sccm respectively, RF power of 80 W, and pressure of 30 mTorr for 360 s**.** A solution of H2O/ 49% HF/ 70% HNO3/ 37% HCl (= 18:2:1:4 by volume) was used to etch the semi elliptical cross section fluidic channel. An etch rate of roughly 1.2 μm/min was observed and half elliptical channels with long diameter 55 μm and short diameter 15 μm were obtained (Figure 2.1 [g]). Acetone was then used to remove the remaining photoresist and Cr etchant used to remove the Cr layer.

In the case of half elliptical cross-section channels, holes were drilled in an unpatterned wafer using a two-step drilling process to prevent wafer shattering. Inlet and outlet holes were first drilled using a Dremel Multipro™ handheld drill and a 0.5 mm drill bit. The holes were then expanded using a 0.9 mm drill bit. In the case of fully elliptical cross section channels, holes were drilled in the same manner on a patterned wafer. In both cases the two wafers were again, cleaned in a Piranha solution then rinsed in DI water and dried thoroughly with N_2. Fully elliptical channels were aligned using a Karl Suss MA-6 Mask Aligner and bonded using Karl Suss SB6 Substrate/Wafer Bonder with the help of Vinh Nguyen at Georgia Tech. Half elliptical channels were bonded according to the same furnace recipe as fully elliptic cross section channels after being removed from the wafer bonder. The two aligned wafers were placed between two flat alumina plates to prevent them from adhering to any fixtures during the bonding process. The plates were then placed in a furnace with a metal weight pressing them together in order to facilitate the desired bonding. The furnace was then heated at a ramp rate of 15 °C/minute to 680 °C and held for 15 minutes, the furnace was then cooled down at a rate of

approximately -2 °C/minute. Finally, 0.99 mm outside diameter plastic tubing was inserted into each drilled hole and sealed with two part liquid epoxy.

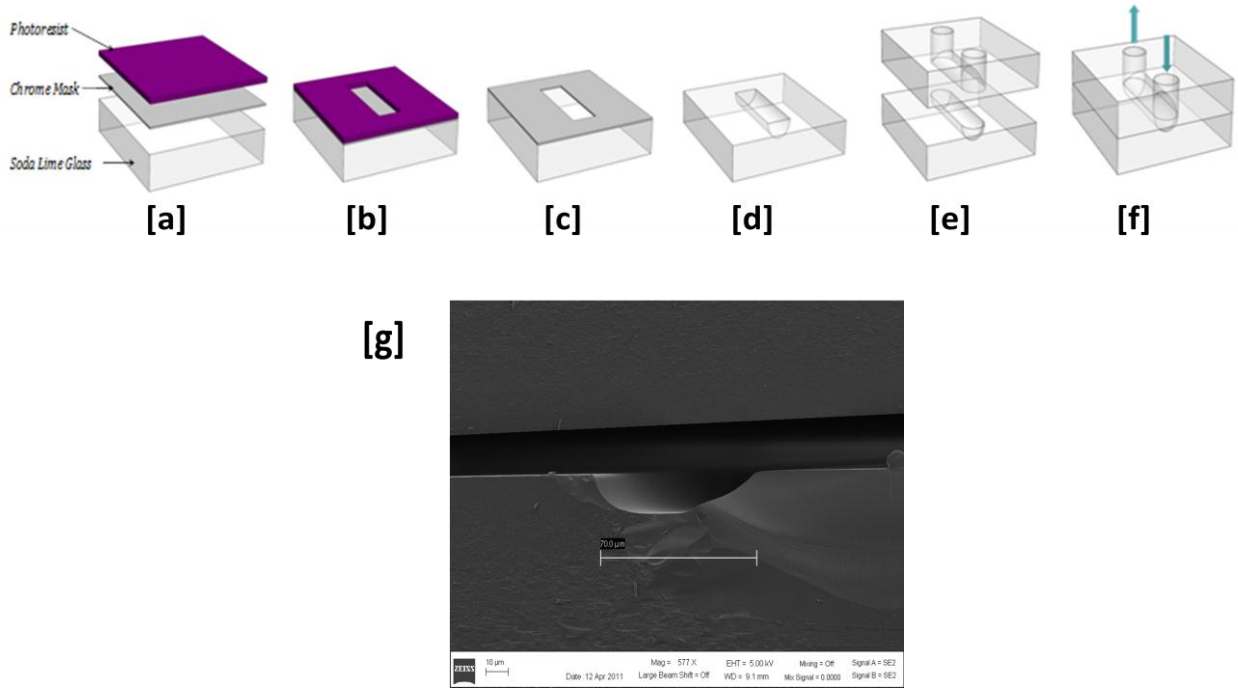

Figure 2.1: Fabrication schematic of fully elliptical cross-section microfluidic channels. Beginning at [a] where layers of Cr and positive photoresist are deposited, then patterned [b]. The glass is then etched using a wet etching process [c] and all masking layers removed [d]. Channels are then aligned [e] and thermally bonded [f] to allow for microfluidic channel flow. [g] Shows a scanning electron microscope (SEM) image of a half channel cross-section.

2.2 Experimental Setup

Image acquisition was performed using an Olympus BX-41 laboratory microscope (Olympus Corporation, USA) containing a filter cube with low pass cut off of 470 nm and hi pass at 500 nm. All fluorescence images were taken using a long working distance 50X objective (Olympus Corporation, USA), Qimaging Retiga-2000RV cooled monochrome camera, and Qcapture Pro software. Fluorescent polystyrene particles presenting surface carboxyl groups were obtained from Bangs Laboratories. Particles with diameters of 970, 780, 390, 210, and 93 nm were used. The particles contained either Dragon Green fluorophore with peak excitation at

480 nm and emission at 520 nm or Fluorescein Isothiocyanate (FITC) with peak excitation at 490 nm and emission at 525 nm incorporated in the particle matrix to produce the fluorescence signal. Solutions of each particle size were made at a concentration of 1 x 10^{10} particles/ml in DI water. The Solutions were then placed in 1 ml syringes with 23 gauge needles attached. The needle was then inserted into the plastic tubing leading to the microfluidic channel. A syringe pump (New Era Pump Systems, NE-1000) controlled the volumetric flow rate and produced a physiologically relevant rate of 25 μl/min [1]. Images were taken of the top wall before the flow, at 1s, and every 20s for a total flow time of 360s. For each image the number of particles adhered to the top wall of the 55 x 120 μm^2 imaged region of the semi-elliptical crossection channel were counted. For smaller sizes, where the number of particles adhering became very large, a particle counting technique based on fluorescence intensity was implored. A region of interest 55 X 15 μm^2 was designated. For the first four images (0, 1, 20, and 40 s) average pixilated intensity profiles were gathered (Figure 2.2 A). The intensity gain from 1 to 20 s and from 20 to 40 s were then correlated to the number of new particles adhered which were counted using the same method as for larger particles. This relation between intensity gain and particle gain was then used to determine new particle adherence for the remaining images. The number of particles in the region of interest was then multiplied by the area of the top wall of the channel in one full image area over that of the region of interest to maintain consistency in the # of particles adhering with other sizes. The Time dependent intensity profiles along with the correlated new particle adherence for that intensity and a representative florescence image showing the region of interest at 20 and 360 s for a single run are shown in Figure 2.2. A sample size of at least 4 for every particle diameter was used and all error bars represent the random uncertainty with a confidence interval of 95%.

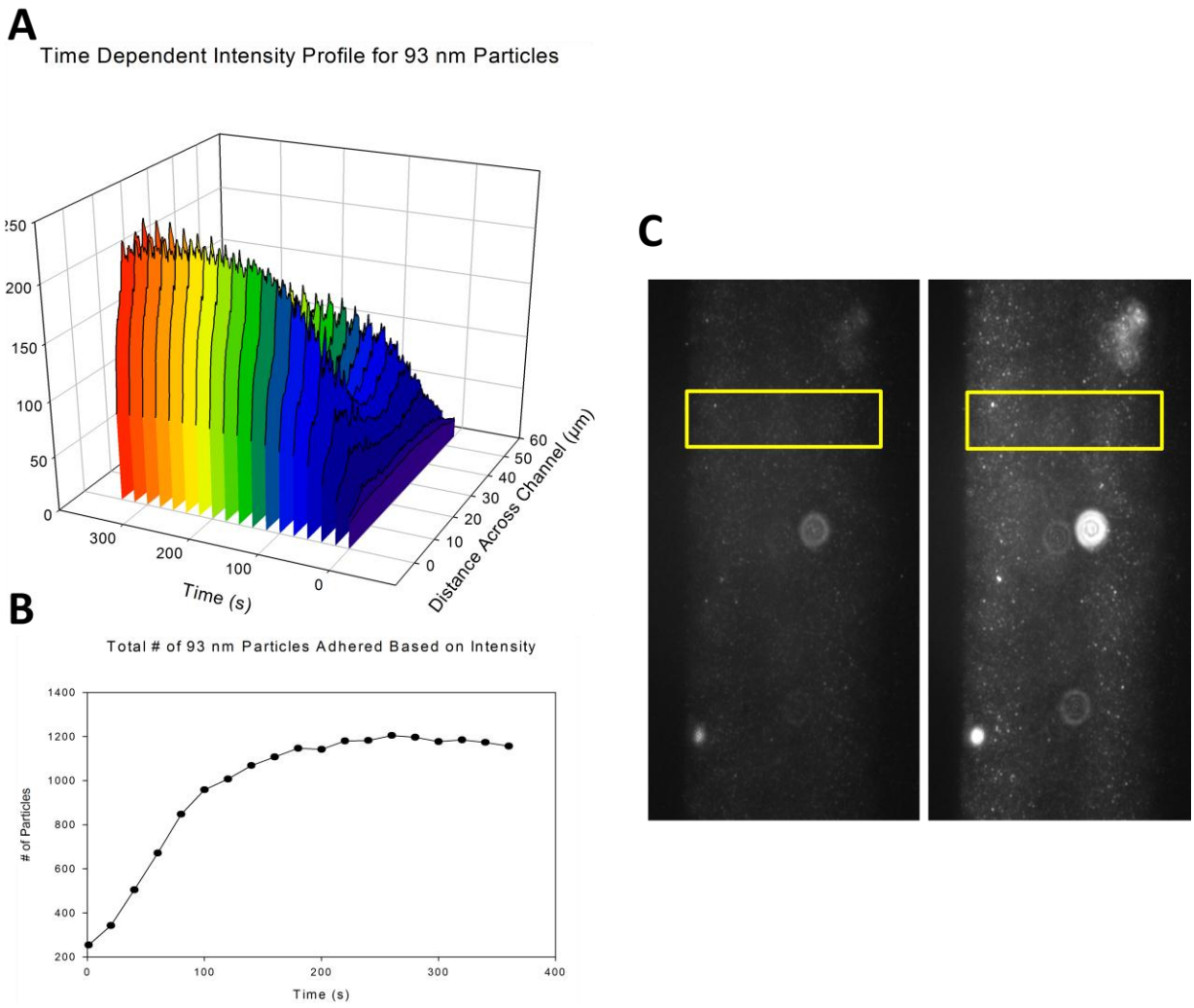

Figure 2.2: [A] Time dependent intensity profiles across the channel section. [B] Total number of particles adhered to the channel wall in the region of interest at each 20s interval for a sample run (360s). [C] Fluorescence images after 20s (left) and 360s (right) of flow with the region of interest (designated by the yellow rectangle) of 93 nm polystyrene spheres.

In order to verify the accuracy of the fluorescence intensity counting method it was used to count the number of particles in a run of larger, 390 nm, particles and juxtaposed with the manual counting method. This was done because 390 nm diameter particles are readily distinguished as individual particles for all time points and would serve as validation of the

method for smaller sizes. Figure 2.3 shows the correlation between the two methods for one run of 390 nm particles.

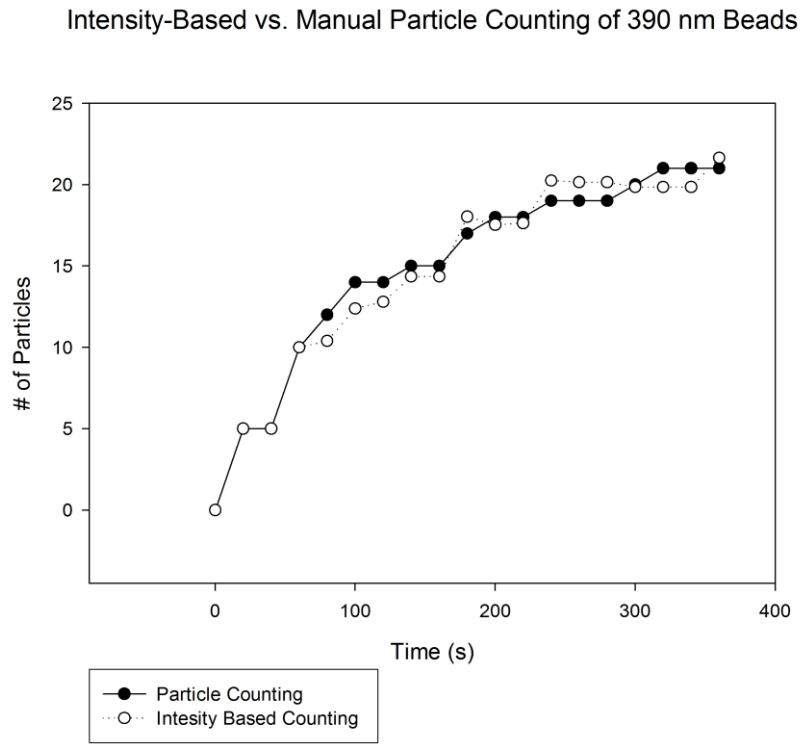

Figure 2.3: Number of 390 nm particles adhered to the imaged surface based on manual counting and intensity quantification methods respectively.

2.3 MANUFACTURING SHAPE-SPECIFIC POLYMERIC NANOPARTICLES

2.3.1 Jet and Flash Imprint Lithography (J-FIL™)

The J-FIL™ process was used to manufacture shape-specific polymeric nanoparticles with characteristic dimensions as low as 50 nm. A standard quartz master template, with the desired feature shape and size, was coated with a self assembled monolayer (SAM) of 0.5% (v/v) (Tridecafluoro-1,1,2,2-Tetra-Hydrooctyl) Dimethylchloro-silane (Gelest Inc,) in toluene and used to make the template surface non-adhesive and suitable for nanoimprinting. The template was manufactured using standard template manufacturing processes including electron beam

lithography (EBL) [51]. The UV nanoimprints were carried out on 8 in. silicon wafers spincoated with a back anti-reflective coating (DUV 30J-6, 3000 rpm, 60s), followed by a top layer of 2% (w/v) poly(vinyl alcohol) (PVA, 31kDa m, Fluka) (2500 rpm, 60s). Nanoimprinting was performed using an Imprio® 100 (Molecular Imprints Inc.) where a piezoelectric single point dispense tip dispensed the required amount of imprtintable macromer solution onto the wafer. Imprintable macromer volumes as low as 8 nL for one 5mm x 5mm imprint region are dispensed to imprint and produce ~1.5 x 10^9 particles. Figure 2.4 shows a schematic of the J-FIL™ process. In order to isolate the imprinted particles, the residual layer between the nanoparticles was removed by a 20–90 s oxygen plasma etch using an Oxford PlasmaLab 80 RIE™ Series reactive ion etcher (RIE). The imprinted nanoparticles were then released by applying filtered DI water on the wafer to dissolve the water soluble PVA release layer.

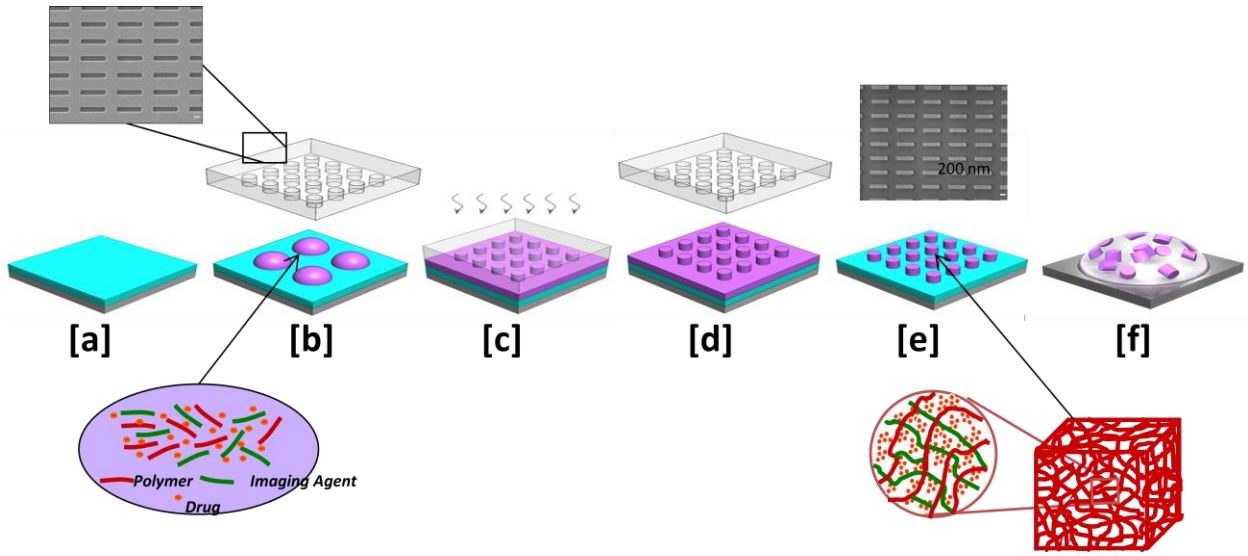

Figure 2.4: Jet and Flash Imprint lithography (J-FIL™) process: [a] Spin coat sacrificial PVA layer onto Si wafer [b] Inkjet bio-solution containing photo crosslinkable polymer and drug and/or imaging agent and align template [c] Imprint and UV cure solution [d] Release template [e] Etch residual layer [f] Dissolve PVA layer, releasing particles into solution [51]. (Scale bar = 200 nm)

Figure 2.5 shows an SEM image of released 250 X 125 nm cylindrical particles as well as a fluorescent image obtained through soda lime glass wafers on the imaging setup described above.

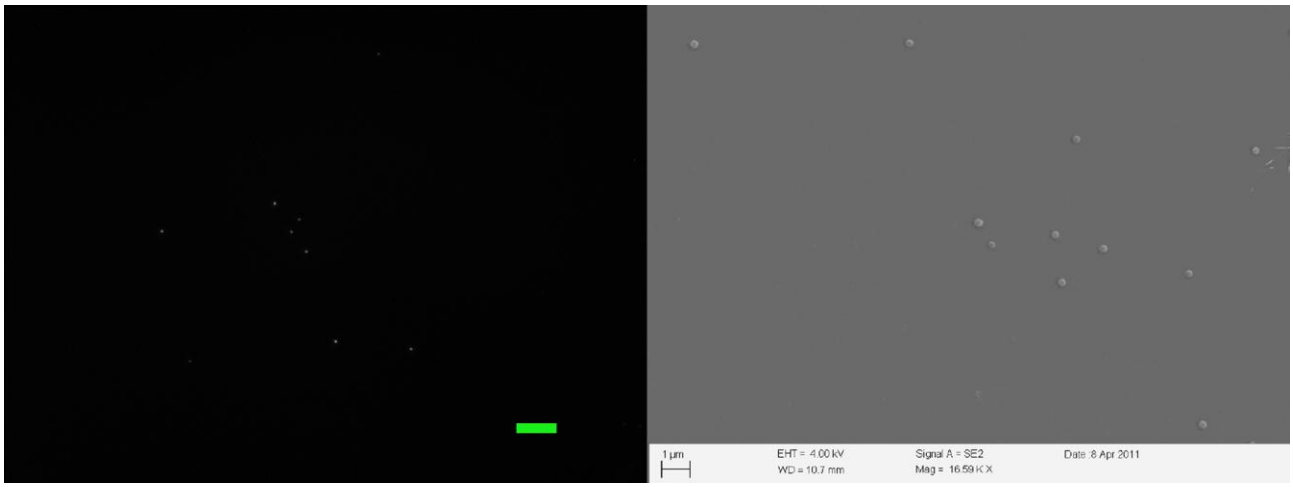

Figure 2.5: Left, Fluorescence image of FITC encapsulated PEGDA nanoparticles (Scale bar = 5 µm). Right, SEM image of 250 X 125 nm cylindrical FITC encapsulated PEGDA nanoparticles.

Chapter 3: Experimental Results and Discussion

3.1 Results

Figure 3.1 shows a typical image at 360s for each of the particle sizes. In each case the trial began at t = 0 with no particles adhered to the top wall. At t = 1 s an interesting phenomenon occurred where, due to capillary pressure and wetting phenomena an initial particle deposition of some number of particles was observed and not thought to be relevant to the study of steady state particle margination and adherence propensity. The data in Figure 3.1 shows the total number of particles adhered after 360 s of flow for each size subtracting that initial deposition and the error bars represent the random uncertainty, with a 95% confidence interval. The number of 970 nm particles was found to be zero and thus does not show up on this plot as the y-axis is log scale.

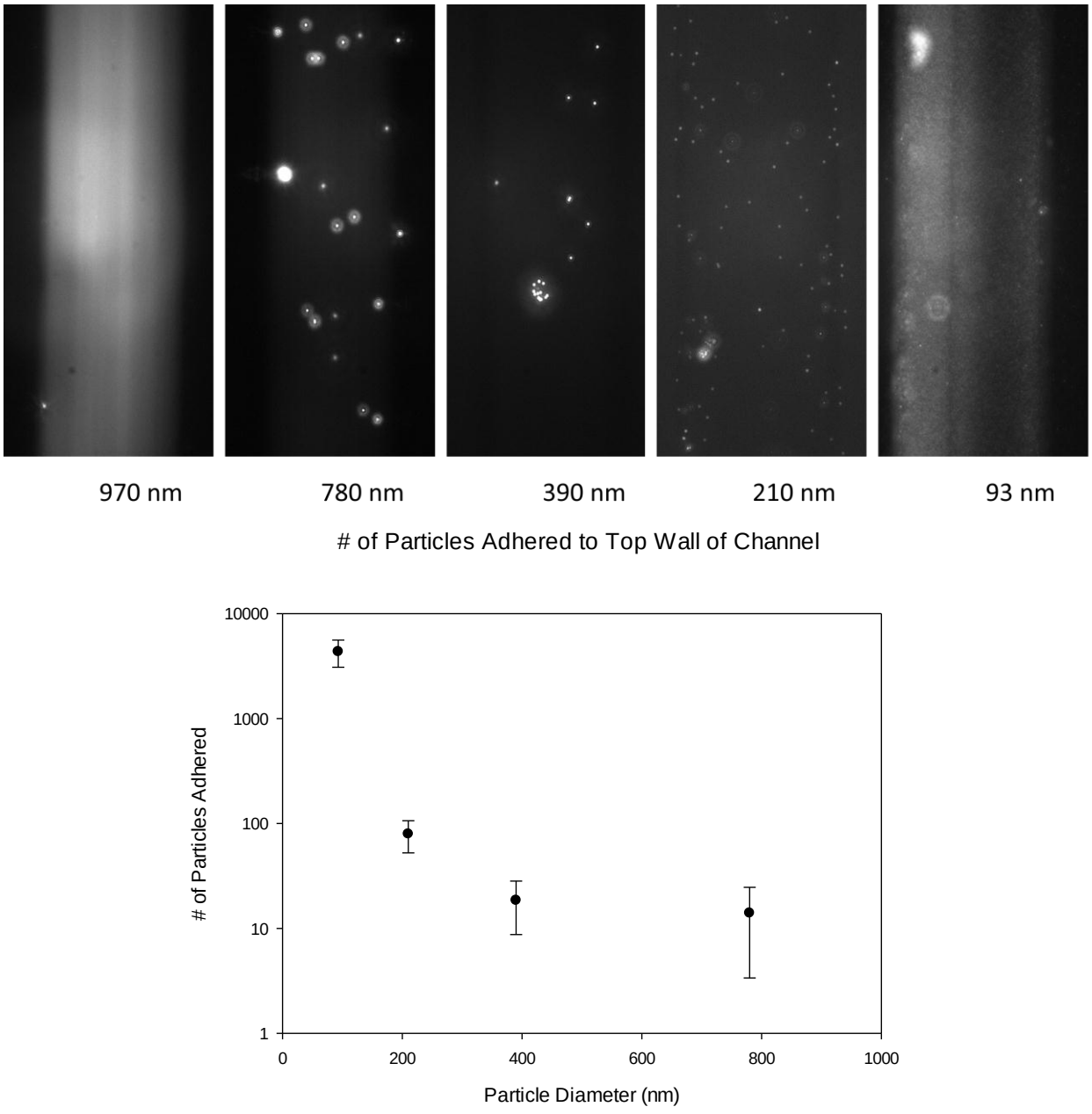

Figure 3.1: [Top] Representative fluorescence images after 360 s of continuous particle flow for each size respectively (all channels are 55 μm in width). [Bottom] # of particles adhered after 360 s of flow for each size. Error bars indicate the random uncertainty with a confidence interval of 95%.

For a single particle size the general time dependent particle saturation trend observed was consistent across trials as well as with that observed in previous particle deposition studies

[32, 47]. After some time of sustained new particle deposition, the surface eventually became saturated and no new particles adhered to the wall (Figure 3.2).

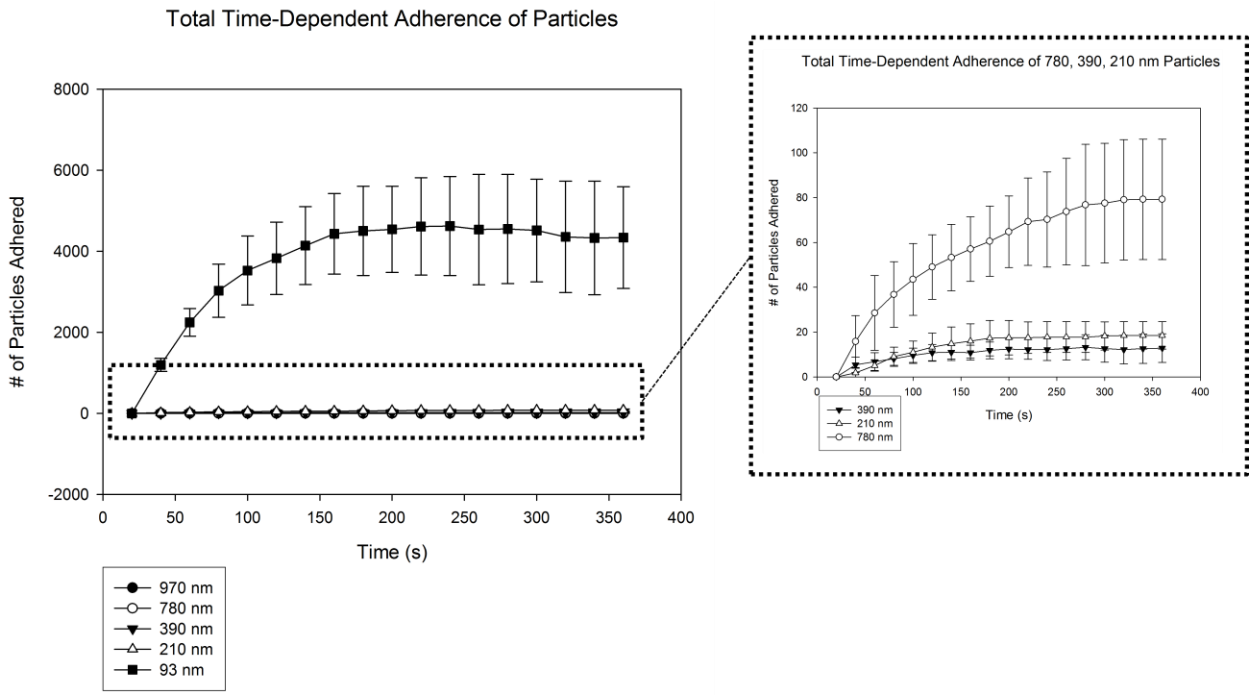

Figure 3.2: Particle saturation curves showing no new particle adherence at 360s.

From the total adhered particle data, deposited particle volume per unit area in each image was calculated by multiplying the number of particles adhered to the surface by the volume of a single particle of the given size. The volume delivery efficiency, or total volume of particles adhered to the wall per image area versus the total volume of particles injected, for each particle size is plotted in Figure 3.3**.** The total volume of injected particles was calculated using a simple mass balance and the experimental parameters provided. The insert is the same adhered particle volume data plotted against particle diameter.

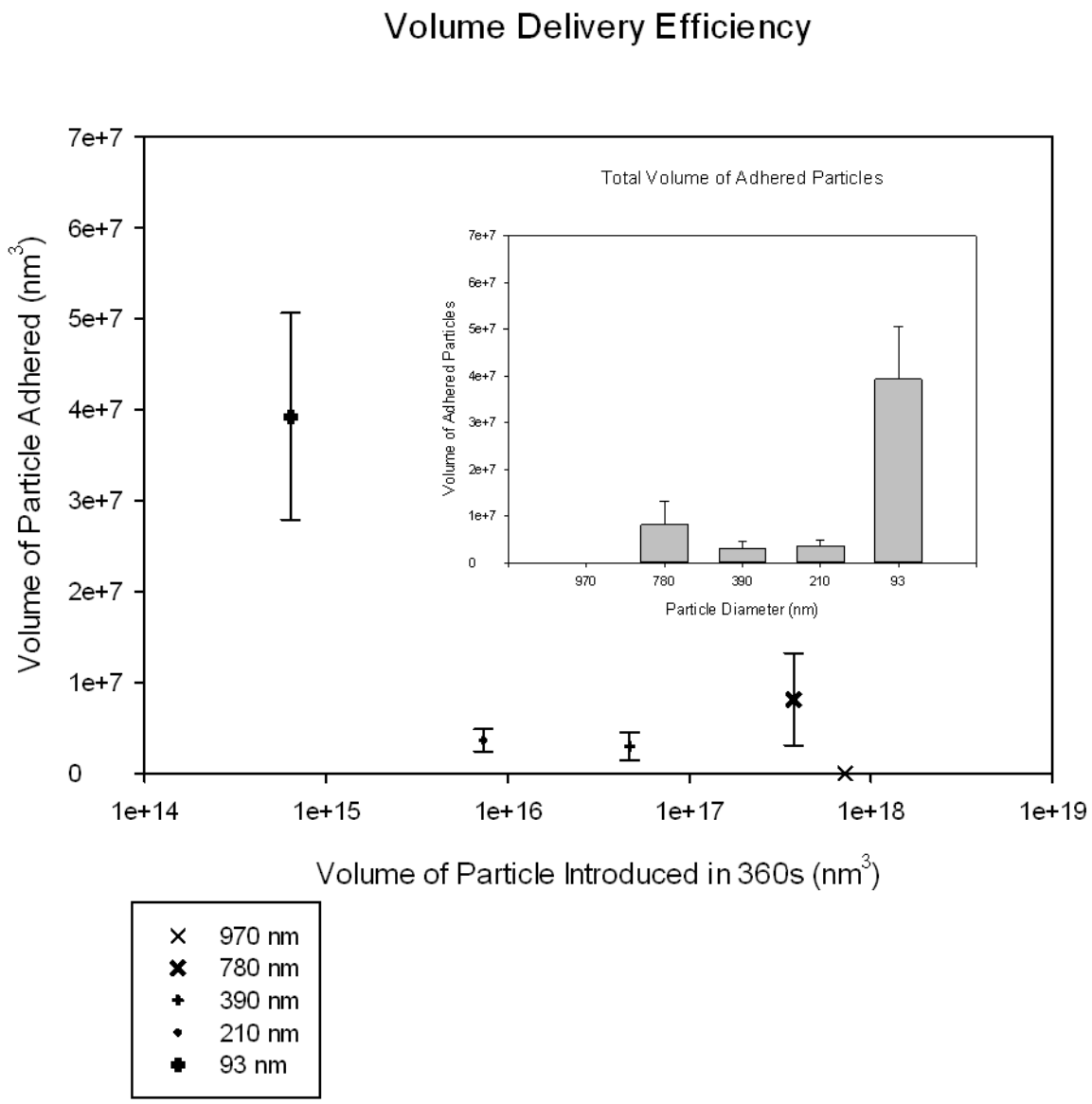

Figure 3.3: Volume delivery efficiency of each particle size. Insert: Total volume of particles adhered to the imaged surface of the channel versus particle diameter.

3.2 DISCUSSION

The results show a marked increase in total particle deposition, volume deposition, and deposition efficiency below 200 nm. The relevant forces inducing margination for sub-micron particles are a hemodynamic force acting to keep particles on streamlines given by

$$F_H = \frac{5}{2}\pi\mu d^2\dot{\gamma} \tag{3.1}$$

where $\dot{\gamma}$ is the shear rate, a gravitational force acting perpendicular to the channel wall

$$F_G = \frac{1}{6}\pi d^3 \rho_p g \tag{3.2}$$

and Brownian force acting in a random fashion

$$F_b = 2\frac{k_B T}{d} \tag{3.3}$$

These forces are plotted as a function of particle diameter in Figure 3.4. As particle diameter decreases, the effect of gravity (buoyancy) with respect to both hemodynamic forces and diffusive forces is greatly diminished. For 970 nm particles both diffusive and gravitational forces are relevant as margination forces, consistent with the observation of 780 nm particles adhering to the top wall of the channels. One anomalous result is that no 970 nm particles were seen marginating and adhering to the top surface. Given that diffusive and gravitational forces are approximately equal at this particle size, some number of 970 nm particles would be expected to receive enough random bumps due to molecular collisions to marginate toward the top wall as do the 780 nm particles.

In order to unpack this behavior let us first consider the relative importance of shear flow and particle inertia. For polystyrene particles in water ($\mu = 10^{-3}\ Pa \cdot s$, $\Delta\rho = 50\ kg/m^3$, $\rho_f = 10^3\ kg/m^3$) and the experimental parameters described above, the mean flow velocity is given by

$$U_m = \frac{Q}{A} = 0.325\ \frac{m}{s} \tag{3.4}$$

where Q is the volumetric flow rate and A is the channel cross sectional area. The dimensionless quantities describing the contributions of buoyancy and relative importance of shear flow and particle inertia respectively are much less than unity and given by:

$$\frac{\alpha^2}{B} = \frac{9}{2}\frac{\mu U_m}{h^2 \Delta \rho g} < O(10^{-1}) \tag{3.5}$$

and

$$Re_{channel} B^2 = \frac{1}{18} R_{h,c} d^2 \frac{\rho_f \Delta \rho g}{\mu^2} \ll O(10^{-1}) \tag{3.6}$$

for all particle sizes considered. This corresponds to the regime in which shear inertia is dominant and spherical particles drift to an equilibrium position close to the wall (Table 2). This predicts an increasingly marginated equilibrium position with particle diameter but says nothing of the adhesion antipathy of 970 nm particles.

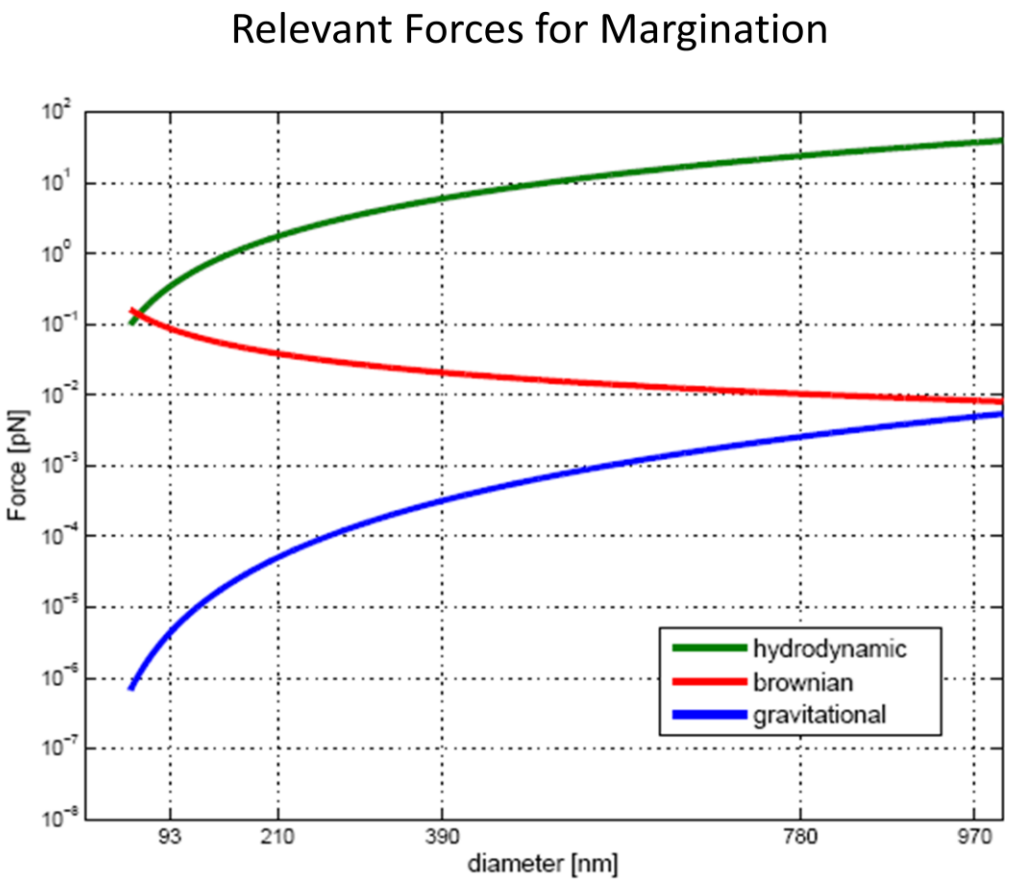

Figure 3.4: Plot of relevant marginating forces at sub-micron particle diameters.

Having shown that there is no special bulk flow phenomenon to explain the precipitous drop in 970 nm particle margination and adherence propensity let us now look more closely at adhering forces. There are two regimes to consider in a particles journey to adherence. The first is a region in which the particle has marginated sufficiently close to the wall and exhibits a "jump into contact" behavior due to van der Waals interactions first described by Decuzzi *et al*. The distance from the wall, h, in which van der Waals interactions dominate margination depends on several factors discussed above, but is typically in the range of 2 to 10 particle diameters for sub micron particles [37]. The second region is the near-wall region, typically h = 10 nm where other nanoscale forces begin to dominate particle motion. The complex nature of electrostatic and steric interactions at separation distances less than 10 nm are not considered here but for an adhering particle, would tend to be large for small h and influenced readily by the surface to volume ratio of the particle [38]. The lift force for a spherical particle in contact with a flat surface was computed by Zeng *et al.* and shown to fall off rapidly as the gap between the particle and the wall increases from a contact position[52]. However these colloidal fluid phenomena are also dependent on a number of factors including flow Reynolds number and geometric considerations. The physical reality is that, at the wall, electrostatic repulsion due to the formation of the electric double layer, steric and salvation forces, as well as colloidal pressures repel the particle sufficiently that a rigorous estimation of the near-wall adhesion force is elusive. For a circulating particle, Decuzzi *et al.* showed –considering the contribution of buoyancy, hemodynamic forces, van der Waals, electrostatic and steric interactions- that only buoyancy, hemodynamic forces, and van der Waals interactions need be considered at separation distances of more than 10 nm [37]. Removing the complexity of near-wall phenomena, the attractive force on the particle due solely to van der Waals interaction can be calculated from

interaction energy between a spherical particle and a flat plate given in equation 1.16 and having d^3 and h^{-4} dependence.

This *back of the envelope* calculation for a marginating force shows that larger particles should be attracted to the wall considerably more than smaller ones for moderate separation distances and more so at small separation distances. Experimental results indicate that a critical particle diameter for firm adhesion exists wherein the relevant adhesive and repulsive forces result in particle detachment. For every unique particle-wall-medium material composition and shear rate this critical diameter can be determined. For the experimental setup discussed here the critical diameter for adhesion seems to lie between 780 nm and 970 nm and further experimental results for particles sizes between these two values would bring the critical diameter into finer focus. *Decuzzi et al.* reported a scaling relationship between a critical shear stress for silica beads with (1 μm $< d <$ 5 μm) of $\mu\dot{\gamma}_{critical} \propto d^{-1.35}$ [49]. This relationship shows that, for silica beads in a parallel plate flow chamber, the shear detachment force grows more rapidly with diameter than does the nonspecific adhesion force which also appears to be the case in the current setup. Further flow tests varying the shear rate would need to be performed to obtain a similar relation. For engineered nanocarriers, determination of this critical shear stress would be of paramount importance in efficient rational design.

At particle diameters below 100 nm the diffusive forces are approximately equal to any hydrodynamic force away from the wall (Figure 3.4). This relation, wherein Brownian collisions are sufficient to knock particles off of inertial streamlines gives rise to a regime in which diffusive margination is dominant. Noting that total adherence in 93 nm particles is increased by orders of magnitude over particles not in the diffusion dominated margination regime may be of value in further rational design of particle based drug delivery.

Given that nanoparticle volume here is directly analogous to drug loading capacity in nanocarriers, and that the cost of some cancer drugs is prohibitively expensive for many research budgets [53] volume delivery efficiency may be an important metric. While there are still a myriad of factors that determine whether or not a particle ultimately ends up in a targeted cell, certainly one prohibitive characteristic is low margination and adhesion propensity. Reducing particle diameter from 780 nm to 93 nm in this work resulted in a fourfold gain in volume delivery efficiency. Increasing this efficiency in an increasingly biomimetic flow experiment may offer a cost effective optimization method for researchers in the rational design of nanocarriers for specific diseases.

Chapter 4: Conclusions and Future Work

Particle size, shape, surface chemistry, and modulus of elasticity, as well as environmental factors such as vessel diameter, wall shear rate, red blood cell interaction, and channel orientation have all been shown to affect transport and adhesion of nano and/or micro particles. An experimental method is described in this thesis to quantify the margination and adhesion propensity of fluorescent nanoparticles. Unique to this method are the ability to count individual nanoparticles, isolate and image the top wall of the flow channel, as well as implementation of channel diameters mimetic of human microcirculation where drug delivery to turmeric cancer cells ultimately takes place. A drastic increase in particle margination was observed as spherical particle diameter decreased. The volume delivery efficiency, or ratio of total adhered particle volume to total injected particle volume, increased by a factor of four from 780 nm particles to 93 nm particles. At increasingly small particle diameters diffusion is shown to be the dominant mechanism for margination and an increase in surface area to volume ratio thought to promote adhesion. Biological landmarks of 500 nm and 200 nm associated with EPR-based delivery strategies and effective MPS avoidance respectively; indicate a need for sub 200 nm nanoparticle transport characterization.

The major advantage of *in-vitro* characterization of nanoparticle margination and adhesion propensity over *in-vivo* biodistribution studies from a nanotherapeutic standpoint, is that very few particles are required compared to *in-vivo* studies. Numerical models used to predict margination and adhesion propensity of nano and micro particles have shown that the oscillating trajectory of non-spherical nanoparticles caused by particle tumbling may result in net lateral drift or large enough oscillations to explore biophysical diversities such as targeted receptors or tumeric fenestrations. This marginating behavior has been shown both

experimentally and numerically to increase with particle aspect ratio for microparticles. However the applicability of these methods to complex vessel architecture and diverse particle geometries is a limiting factor. Given the difficulty associated with manufacturing size and shape-specific polymeric nanoparticles and the shortcomings of current numerical methods, experimental throughput is an important consideration. The ability to readily manufacture geometrically mimetic microfluidic channels also facilitates the characterization of nanoparticle margination and adhesion propensity varying any number of relevant factors. Ergo facilitating a better understanding of delivery strategies for complex diseases where for example, abnormally high shear rates may be involved. From a fundamental transport perspective, the unique ability to visualize sub-100 nm particles on a single channel side could provide insight into the directionally preferential margination propensities of nanocarriers.

Using our J-FIL™ method to fabricate shape-specific polyermeric nanoparticles, a significant library of sub 200 nm particles can be manufactured in sufficient quantities to perform *in-vitro* flow experiments and fluorescently imaged on an individual particle basis. Assailable hurdles exist in functionalizing PEGDA particles to adhere to channel walls but significant progress is being made. Incorporating aminoacrylate groups in the macromer imprinting solutions should allow for surface ligand conjugation and, with proper channel functionalization, specific adherence of polymeric nanocarriers to channel walls. In addition, the effect of aspect ratio on the adhesion and margination propensity of gold nanorods is also within reach. Coating channel walls with fibronectin has been used previously to investigate the difference in adhesion of sub 50 nm gold nanoparticles [32]. However only 50 nm spheres and nanorods with an aspect ratio of 2.2 were explored and further elucidation of the effect of aspect ratio on margination and adhesion propensity is warranted, particularly in small channels

mimetic of human microcirculation. The focused analysis afforded by *in-vitro* flow setups will be needed in conjunction with numerical modeling, as well as *in-vivo* characterizations to facilitate the rational engineering of nanoparticles for the preferential delivery therapeutic agents to targeted cells.

References

1. Barrett, K., Barman, S., Boitano, S., and Brooks, H., *Ganong's Review of Medical Physiology*. 23rd ed.; McGraw Hill: 2010.
2. R. Fahraeus, T. L., "The viscosity of the blood in narrow capillary tubes," *American Journal of Physiology* **96**, 562–568 (1931).
3. G. Bugliarello, J. S., "Velocity distribution and other characteristics of steady and pulsatile blood flow in fine glass tubes," *Biorheology*, 85–107 (1970).
4. Reinke, W., Gaehtgens, P., and Johnson, P. C., "Blood-Viscosity in Small Tubes - Effect of Shear Rate, Aggregation, and Sedimentation," *American Journal of Physiology* **253**, H540-H547 (1987).
5. Sharan, M. and Popel, A. S., "A two-phase model for flow of blood in narrow tubes with increased effective viscosity near the wall," *Biorheology* **38**, 415-428 (2001).
6. NIH National Library of Medicine - Medical Subject Headings. http://www.nlm.nih.gov/cgi/mesh/2011/MB_cgi?mode=&term=Mononuclear+Phagocyte+System (6/14/2001),
7. Singh, I., *Textbook of human histology*. Jaypee Brothers Publishers: 2006.
8. Matsumura, Y. and Maeda, H., "A New Concept for Macromolecular Therapeutics in Cancer-Chemotherapy - Mechanism of Tumoritropic Accumulation of Proteins and the Antitumor Agent Smancs," *Cancer Research* **46**, 6387-6392 (1986).
9. Drummond, D. C., Meyer, O., Hong, K. L., Kirpotin, D. B., and Papahadjopoulos, D., "Optimizing liposomes for delivery of chemotherapeutic agents to solid tumors," *Pharmacological Reviews* **51**, 691-743 (1999).
10. Sergeeva, A., Kolonin, M. G., Molldrem, J. J., Pasqualini, R., and Arap, W., "Display technologies: Application for the discovery of drug and gene delivery agents," *Advanced Drug Delivery Reviews* **58**, 1622-1654 (2006).
11. Neri, D. and Bicknell, R., "Tumour vascular targeting," *Nature Reviews Cancer* **5**, 436-446 (2005).
12. Decuzzi, P., Pasqualini, R., Arap, W., and Ferrari, M., "Intravascular Delivery of Particulate Systems: Does Geometry Really Matter?," *Pharmaceutical Research* **26**, 235-243 (2009).
13. Goldsmith, H. L. and Spain, S., "Margination of Leukocytes in Blood-Flow through Small Tubes," *Microvascular Research* **27**, 204-222 (1984).
14. Schonberg, J. A. and Hinch, E. J., "Inertial Migration of a Sphere in Poiseuille Flow," *Journal of Fluid Mechanics* **203**, 517-524 (1989).
15. Mclaughlin, J. B., "The Lift on a Small Sphere in Wall-Bounded Linear Shear Flows," *Journal of Fluid Mechanics* **246**, 249-265 (1993).
16. Goldman, A. J., Cox, R. G., and Brenner, H., "Slow Viscous Motion of a Sphere Parallel to a Plane Wall .I. Motion through a Quiescent Fluid," *Chemical Engineering Science* **22**, 637-& (1967).
17. Decuzzi, P. and Ferrari, M., "The role of specific and non-specific interactions in receptor-mediated endocytosis of nanoparticles," *Biomaterials* **28**, 2915-2922 (2007).

18. Hogg, A. J., "The Inertial Migration of Non-Neutrally Buoyant Spherical-Particles in 2-Dimensional Shear Flows," *Journal of Fluid Mechanics* **272**, 285-318 (1994).
19. Vasseur, P. and Cox, R. G., "Lateral Migration of Spherical-Particles Sedimenting in a Stagnant Bounded Fluid," *Journal of Fluid Mechanics* **80**, 561-591 (1977).
20. Cozensroberts, C., Quinn, J. A., and Lauffenburger, D. A., "Receptor-Mediated Adhesion Phenomena - Model Studies with the Radial-Flow Detachment Assay," *Biophysical Journal* **58**, 107-125 (1990).
21. Patil, V. R. S., Campbell, C. J., Yun, Y. H., Slack, S. M., and Goetz, D. J., "Particle diameter influences adhesion under flow," *Biophysical Journal* **80**, 1733-1743 (2001).
22. Bell, G. I., Dembo, M., and Bongrand, P., "Cell-Adhesion - Competition between Nonspecific Repulsion and Specific Bonding," *Biophysical Journal* **45**, 1051-1064 (1984).
23. Decuzzi, P., Gentile, F., Granaldi, A., Curcio, A., Causa, F., Indolfi, C., Netti, P., and Ferrari, M., "Flow chamber analysis of size effects in the adhesion of spherical particles," *International Journal of Nanomedicine* **2**, 689-696 (2007).
24. Moghimi, S. M., Hunter, A. C., and Murray, J. C., "Nanomedicine: current status and future prospects," *Faseb Journal* **19**, 311-330 (2005).
25. Conner, S. D. and Schmid, S. L., "Regulated portals of entry into the cell," *Nature* **422**, 37-44 (2003).
26. Gary, D. J., Puri, N., and Won, Y. Y., "Polymer-based siRNA delivery: Perspectives on the fundamental and phenomenological distinctions from polymer-based DNA delivery," *Journal of Controlled Release* **121**, 64-73 (2007).
27. Oupicky, D., Konak, C., Ulbrich, K., Wolfert, M. A., and Seymour, L. W., "DNA delivery systems based on complexes of DNA with synthetic polycations and their copolymers," *Journal of Controlled Release* **65**, 149-171 (2000).
28. Gentile, F., Curcio, A., Indolfi, C., Ferrari, M., and Decuzzi, P., "The margination propensity of spherical particles for vascular
targeting in the microcirculation," *Nanobiotechnology* **6**, (2008).
29. Koutsiaris, A. G., Tachmitzi, S. V., Batis, N., Kotoula, M. G., Karabatsas, C. H., Tsironi, E., and Chatzoulis, D. Z., "Volume flow and wall shear stress quantification in the human conjunctival capillaries and post-capillary venules in vivo," *Biorheology* **44**, 375-386 (2007).
30. Nagaoka, T. and Yoshida, A., "Noninvasive evaluation of wall shear stress on retinal microcirculation in humans," *Investigative Ophthalmology & Visual Science* **47**, 1113-1119 (2006).
31. Charoenphol, P., Huang, R. B., and Eniola-Adefeso, O., "Potential role of size and hemodynamics in the efficacy of vascular-targeted spherical drug carriers," *Biomaterials* **31**, 1392-1402 (2010).
32. Toy, R., Hayden, E., Shoup, C., Baskaran, H., and Karathanasis, E., "The effects of particle size, density and shape on margination of nanoparticles in microcirculation," *Nanotechnology* **22**, - (2011).
33. Tao, L., Hu, W., Liu, Y. L., Huang, G., Sumer, B. D., and Gao, J. M., "Shape-specific polymeric nanomedicine: emerging opportunities and challenges," *Experimental Biology and Medicine* **236**, 20-29 (2011).
34. Jeffery, G. B., "The Motion of Ellipsoidal Particles Immersed in a Viscous Fluid," *Proc. R. Soc. Lond. A* **102**, 161-179 (1922).

35. Han, Y., Alsayed, A. M., Nobili, M., Zhang, J., Lubensky, T. C., and Yodh, A. G., "Brownian motion of an ellipsoid," *Science* **314**, 626-630 (2006).
36. Decuzzi, P., Lee, S., Decuzzi, M., and Ferrari, M., "Adhesion of microfabricated particles on vascular endothelium: A parametric analysis," *Annals of Biomedical Engineering* **32**, 793-802 (2004).
37. Decuzzi, P., Lee, S., Bhushan, B., and Ferrari, M., "A theoretical model for the margination of particles within blood vessels," *Annals of Biomedical Engineering* **33**, 179-190 (2005).
38. Israelachvili, J. N., *Intermolecular and Surface Forces*. 3rd ed.; Academic Press: 2011.
39. Lee, S. Y., Ferrari, M., and Decuzzi, P., "Shaping nano-/micro-particles for enhanced vascular interaction in laminar flows," *Nanotechnology* **20**, - (2009).
40. Peskin, C. S. and Mcqueen, D. M., "A 3-Dimensional Computational Method for Blood-Flow in the Heart .1. Immersed Elastic Fibers in a Viscous Incompressible Fluid," *Journal of Computational Physics* **81**, 372-405 (1989).
41. Hu, H. H., Patankar, N. A., and Zhu, M. Y., "Direct numerical simulations of fluid-solid systems using the arbitrary Lagrangian-Eulerian technique," *Journal of Computational Physics* **169**, 427-462 (2001).
42. Zhang, L., Gerstenberger, A., Wang, X. D., and Liu, W. K., "Immersed finite element method," *Computer Methods in Applied Mechanics and Engineering* **193**, 2051-2067 (2004).
43. Liu, W. K., Liu, Y. L., Farrell, D., Zhang, L., Wang, X. S., Fukui, Y., Patankar, N., Zhang, Y. J., Bajaj, C., Lee, J., Hong, J. H., Chen, X. Y., and Hsua, H., "Immersed finite element method and its applications to biological systems (vol 195, pg 1722, 2006)," *Computer Methods in Applied Mechanics and Engineering* **195**, 4655-4655 (2006).
44. Liu, Y. L. and Liu, W. K., "Rheology of red blood cell aggregation by computer simulation," *Journal of Computational Physics* **220**, 139-154 (2006).
45. Shah, S., Liu, Y. L., Hu, W., and Gao, J. M., "Modeling Particle Shape-Dependent Dynamics in Nanomedicine," *Journal of Nanoscience and Nanotechnology* **11**, 919-928 (2011).
46. Geng, Y., Dalhaimer, P., Cai, S. S., Tsai, R., Tewari, M., Minko, T., and Discher, D. E., "Shape effects of filaments versus spherical particles in flow and drug delivery," *Nature Nanotechnology* **2**, 249-255 (2007).
47. Gentile, F., Chiappini, C., Fine, D., Bhavane, R. C., Peluccio, M. S., Cheng, M. M. C., Liu, X., Ferrari, M., and Decuzzi, P., "The effect of shape on the margination dynamics of non-neutrally buoyant particles in two-dimensional shear flows," *Journal of Biomechanics* **41**, 2312-2318 (2008).
48. Doshi, N., Prabhakarpandian, B., Rea-Ramsey, A., Pant, K., Sundaram, S., and Mitragotri, S., "Flow and adhesion of drug carriers in blood vessels depend on their shape: A study using model synthetic microvascular networks," *Journal of Controlled Release* **146**, 196-200 (2010).
49. Decuzzi, P., Godin, B., Tanaka, T., Lee, S. Y., Chiappini, C., Liu, X., and Ferrari, M., "Size and shape effects in the biodistribution of intravascularly injected particles," *Journal of Controlled Release* **141**, 320-327 (2010).
50. Merkel, T. J., Jones, S. W., Herlihy, K. P., Kersey, F. R., Shields, A. R., Napier, M., Luft, J. C., Wu, H. L., Zamboni, W. C., Wang, A. Z., Bear, J. E., and DeSimone, J. M., "Using mechanobiological mimicry of red blood cells to extend circulation times of hydrogel

microparticles," *Proceedings of the National Academy of Sciences of the United States of America* **108**, 586-591 (2011).
51. Peppas, N. A., Hilt, J. Z., Khademhosseini, A., and Langer, R., "Hydrogels in biology and medicine: From molecular principles to bionanotechnology," *Advanced Materials* **18**, 1345-1360 (2006).
52. Zeng, L. Y., Najjar, F., Balachandar, S., and Fischer, P., "Forces on a finite-sized particle located close to a wall in a linear shear flow," *Physics of Fluids* **21**, (2009).
53. Fiorino, T., "Industry, clinical trials, and the cost of cancer drugs: An investor's perspective," *Journal of Clinical Oncology* **25**, E21-E23 (2007).